10.1109/ULTSYM.2015.0171

Structure Function: Theory, Ultrasonic Measurement, and Histology

Aiguo Han, *Member*, IEEE, and William D. O'Brien, Jr., *Life Fellow*, IEEE

Department of Electrical and Computer Engineering, University of Illinois, Urbana, IL. e-mail: wdo@uiuc.edu

***Abstract*—Ultrasonic scattering is determined by not only the properties of individual scatterers, but also the correlation among scatterer positions. The role of scatterer spatial correlation is significant for dense medium, but has not been fully understood. The effect of scatterer spatial correlation may be modeled by a structure function (three-dimensional Fourier transform of the scatterer positions) as a frequency-dependent factor in the backscatter coefficient (BSC) expression. To study the structure function, we have performed three steps: 1) we developed theoretical structure function models that take into account the polydispersity of spherical scatterers; 2) we developed the cell pellet biophantom technique to estimate the structure function from ultrasound backscattered data (11 – 105 MHz); 3) we developed algorithms for estimating the structure function from histology, independent of the acoustic measurements. The acoustically estimated and histologically estimated structure functions show consistent frequency dependency, which demonstrates the correlation between acoustically estimated structure function and scatterer position distribution observed in histology. Furthermore, fitting the theoretical polydisperse structure function model to the experimental structure functions yielded relatively accurate cell radius estimates (error < 16%). Our results suggest that the structure function is required for accurately modeling the acoustic scattering in dense medium.**

Keywords*—Structure function; acoustic scattering; dense medium; histology; quantitative ultrasound

I. Introduction

Recent development in quantitative ultrasound (QUS) has expanded to clinical settings for breast cancer treatment monitoring [1], liver fat quantification [2], [3], and breast cancer characterization [4]. For a model-based QUS approach, an acoustic scattering model is fitted to the estimated backscatter coefficient (BSC) to yield parameters that may provide diagnostic information on the tissue microstructure (e.g., scatterer size, shape, and acoustic concentration). For this approach to work, the acoustic scattering model has to be accurate for the investigated tissue.

There are primarily two categories of scattering models in literature: the continuous models that describe the medium as random continua characterized by its fluctuations in density and compressibility [5], [6], and the discrete models that assume the medium is composed of independently and randomly distributed discrete scatterers [7]–[10]. Most models work well for sparse medium, but not for dense medium. It has been suggested that the difficulty of modeling dense medium scattering arises from the spatial correlation among scatterers [11].

Twersky introduced the concept of structure function to the field of acoustic scattering to model the spatial correlation of scatterers [12], [13]. Fontaine et al. first implemented this concept to describe biological scatterers [14]. The structure function has been used for ultrasound blood characterization to address the difficulty of modeling aggregated cells [15], [16]. BSC models incorporating the Percus-Yevick [17] structure function have been evaluated on concentrated physical phantoms [18] and biological phantoms [19]. In those studies, the structure function was not isolated from the BSC to be directly studied. We developed a biophantom technique to isolate the structure function from BSC and directly evaluate the structure function against polydisperse structure function models [20].

Although the structure function has been successfully estimated from the backscatter data, there has been no direct evidence proving that the acoustically estimated structure function is related to the spatial correlation of scatterers. To address this issue, the scatterer position distribution is obtained herein by analyzing histological images. The structure function is then estimated from the obtained scatterer position distributions.

This paper briefly describes in Section II the polydisperse structure function model to be used, and then introduces in Section III the methods for estimating structure functions from ultrasound and histology. The experimental structure functions (acoustic and histological) are then compared to the theoretical model in Section IV.

II. Structure Function Theory

Consider a plane wave of unit amplitude incident on a scattering volume that contains N discrete scatterers. The structure function is defined as

$$S(\mathbf{K}) = \frac{1}{N}\left|\sum_{j=1}^{N} e^{-i\mathbf{K}\cdot\mathbf{r}_j}\right|^2, \qquad (1)$$

The work was supported by National Institutes of Health (R01CA111289 and R01DK106419.

978-1-4799-8182-3/15/$31.00 ©2015 IEEE

where $\mathbf{r}_j$ is the position of the *j*th scatterer, and **K** is the scattering vector whose magnitude is given by $|\mathbf{K}| = 2k\sin(\theta/2)$, where θ is the scattering angle ($\theta = \pi$ for backscattering). $|\mathbf{K}| = 2k$ for backscattering. The BSC is proportional to $S(2k)$.

If the exact position of each scatterer is known, the structure function can be calculated deterministically using (1). Note that the structure function is simply the squared modulus of the Fourier transform of the scatterer positions. Therefore, (1) is useful for numerically calculating the structure function from histology.

If the positions of individual scatterers are unknown, the structure function will be calculated from the distribution function of the scatterers. Different scatterer distribution function models will result in different structure function models. Polydisperse model I that was developed in [20] is used in this study. The model was an extension of the Percus-Yevick model to the polydisperse case, where the scatterers are assumed to be non-overlapping spheres that are polydisperse in size but monodisperse in complex scattering amplitudes. The probability density function of the scatterer radius is assumed to follow a Γ- (Schulz-) distribution with a probability density function [20]

$$f_z(x) = \frac{1}{z!}\left(\frac{z+1}{a}\right)^{z+1} x^z e^{-\frac{(z+1)x}{a}}, \quad z = 0,1,2,\ldots, \quad (2)$$

where *a* is the mean of the scatterer radius, and *z* is the Schulz width factor which is a measure of the width of the distribution (a greater *z* value represents a narrower distribution). The structure function is expressed as a function of mean sphere radius *a*, Schulz width factor *z*, wave number *k*, and sphere volume fraction *η*. The detailed analytical expression of the structure function for the model is available in Appendix A of [20].

III. Methodology

A. Structure Function Estimation from Ultrasound

The experimental procedure for estimating structure function from ultrasound was published in [20] and described briefly herein for completeness. Three cell lines of cell pellet biophantoms were constructed. The biophantoms were composed of a known number of cells clotted in a mixture of bovine plasma (Sigma-Aldrich, St. Louis, MO) and bovine thrombin (Sigma-Aldrich, St. Louis, MO). The three cell lines were Chinese hamster ovary [CHO, American Type Culture Collection (ATCC) #CCL-61, Manassas, VA], 13762 MAT B III (MAT, ATCC #CRL-1666) and 4T1 (ATCC #CRL-2539). The mean cell radii for CHO, MAT, and 4T1 were 6.7, 7.3, and 8.9 μm, respectively [20]. For each cell line, two cell concentrations were constructed, a higher concentration that mimics the situation of dense tissue, and a lower concentration for which the scatterers may be assumed to be uncorrelated (unity structure function). The structure function for the higher-concentration biophantoms was then estimated using

$$S(f) = \frac{\bar{n}_L BSC_H(f)}{\bar{n}_H BSC_L(f)}, \quad (3)$$

where $\bar{n}_L$ and $\bar{n}_H$ represent the number density for the lower and the higher concentrations, respectively, and $BSC_L(f)$ and $BSC_H(f)$ represent the BSC for the lower and the higher concentrations, respectively. The BSC was estimated using a planar reference technique using three single-element, weakly focused transducers that covered the frequency range from 11 to 105 MHz [20].

B. Structure Function Estimation from Histology

Immediately after ultrasonic scanning, the biophantom was placed into a histology processing cassette and fixed by immersion in 10% neutral-buffered formalin (pH 7.2) for a minimum of 12 h for histopathologic processing. The sample was then embedded in paraffin, sectioned, mounted on glass slides and stained with hematoxylin and eosin (H&E).

The H&E stained tissue section was viewed under a light microscope (Olympus BX–51, Optical Analysis Corporation, Nashua, NH, USA). For each tissue slide, a TIF format picture was taken using the digital camera that was connected to the microscope. The magnification of the objective lens was 40X. The digitized image had a size of 1920 × 1920 pixels, with a resolution of 5.72 pixels/μm. Multiple images were analyzed for each cell line. An example of the digitized image is shown in Fig. 1(a).

A custom MATLAB routine was developed to allow manual determination of the nuclear center for each cell on the image (the nuclear center was assumed to represent the scatterer center). The manual determination process was completed by clicking on the nuclear center of the image in MATLAB (Fig. 1(b)). The nuclear center coordinates were automatically recorded (Fig. 1(c)). Then a matrix of the dimension 1920 × 1920 was created. The matrix dimension was the same as the pixel dimension of the original image (Fig. 1(a)). The matrix elements corresponding to nuclear centers were assigned a value of one, while all remaining matrix elements were assigned a value of zero. Next, a circular window (Fig. 1(d)) of radius 960 pixels was applied to the matrix. All elements outside the circle were assigned a value of zero. A fast Fourier transform was then performed on the windowed matrix after zero padding (padded to $2^{14} \times 2^{14}$ pixels). The squared modulus of the 2D Fourier transform, normalized to unity for large wave numbers, is the structure function for all directions (Fig. 1(e)). Because of radial symmetry of the Fourier transformed image (Fig. 1(e)), a radial averaging was performed, which resulted in a structure function that was only dependent on the modulus of the wave number. For backscattering, the spatial frequency *k* was converted to temporal frequency *f* by the relationship $f = kc/(4\pi)$, where *c* was the speed of sound, and was assumed to be 1540 m/s. The resulting structure function as a function of temporal frequency was the final structure function estimated from histology (Fig. 1(f)).

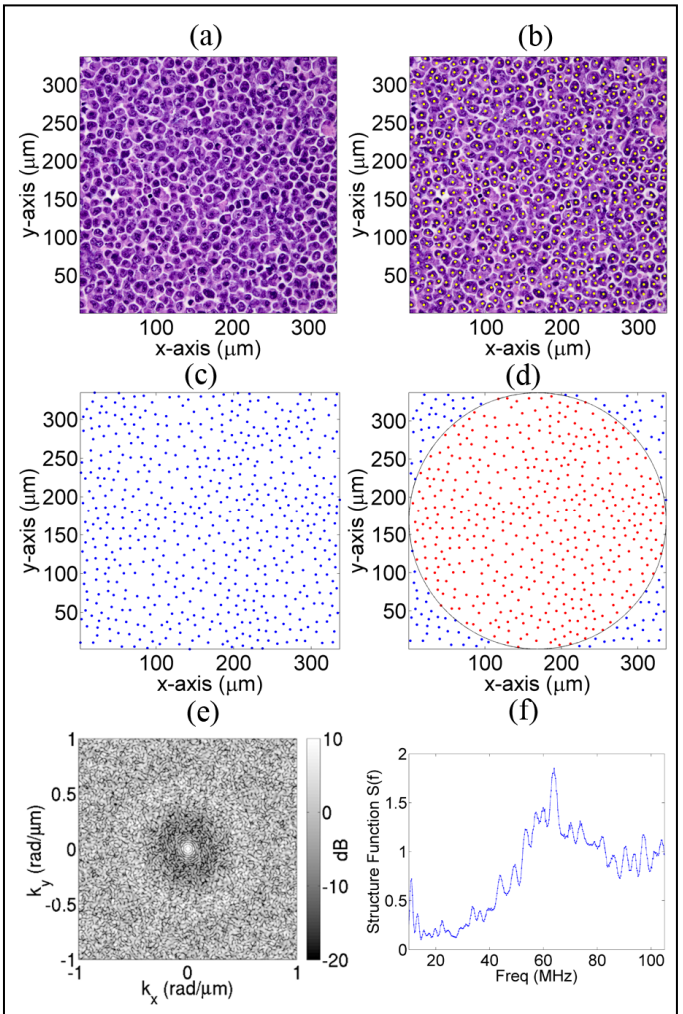

Fig. 1. Step-by-step procedure for estimating the structure function from histology: (a) original H&E image; (b) scatterer positions determined from the H&E image; (c) scatterer positions plotted separately; (d) circular windowing; (e) squared modulus of the 2D Fourier transform of the windowed scatterer positions; (f) final estimated structure function versus frequency. The data shown herein were from a 4T1 cell pellet biophantom sample.

IV. Results and Discussions

The histologically estimated structure function curves are presented in Fig. 2 for high-concentration (74% volume fraction; see Table I of [20] for further details) cell pellet biophantoms of three cell lines: CHO, MAT, and 4T1. Each of the curves was the average of three realizations (i.e., measurements from three different images). Also presented are the acoustically estimated curves published in [20].

None of the curves in Fig. 2 is constant (= 1) across the frequency range plotted. This suggests that the scatterer position distribution does have an influence on the backscattered power spectrum. The scatterer position distributions for these high-concentration biophantoms exhibit similarly destructive interference effects around 30 MHz and constructive interference effects around 70 MHz. These results are expected, because the cells are tightly packed in the high-

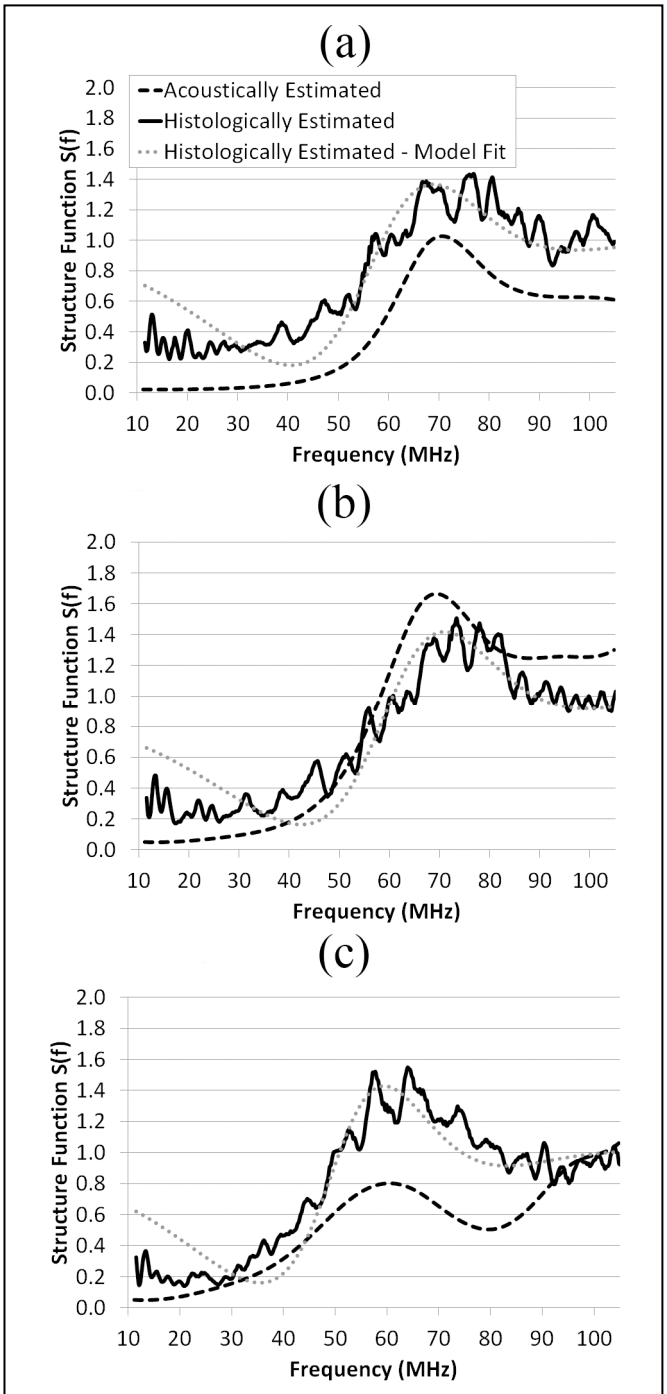

Fig. 2. Comparison between the acoustically estimated (dashed lines) and histologically estimated (solid lines) structure function curves for high-concentration (a) CHO, (b) MAT, and (c) 4T1 cell pellet biophantoms. Also presented are the best-fit structure functions to the histologically estimated curves using a polydisperse structure function model. The dashed curves were adapted from the experimental curves of Fig. 7 in [20].

concentration biophantoms such that the scatterer positions are highly correlated. The correlation should be related to the cell diameters. Theoretically, a larger scatterer diameter corresponds to a lower constructive frequency if the scatterers are tightly packed. Fig. 2 shows that the 4T1 has the lowest peak frequency in the structure function curve out of the three

cell lines, which is consistent with the fact that 4T1 has the largest cell radius out of the three.

The general trends of the acoustically estimated and histologically estimated curves appear to be similar for all the cell lines. The peak positions agree well (within 5 MHz) between the two structure function curves for each of the three cell lines. The magnitude agreement is not as good, however. Only MAT shows reasonable agreement in structure function curves (Fig. 2(b)). For CHO, the acoustically estimated structure function is mostly lower than the histologically estimated structure function across the frequency range (Fig. 2(a)). The peak magnitude barely exceeds unity for the acoustically estimated structure function for CHO. The 4T1 appears to behave similarly in magnitude to that of the CHO, i.e., the peak magnitude is less than unity.

A number of reasons might have contributed to the magnitude discrepancy. Errors in the number density estimation can result in errors in the magnitude of the ultrasonically estimated structure function. Also, 2D histology does not perfectly represent the 3D situation. Further, the fixing processing introduces slight cell shrinkage.

Despite the discrepancy in magnitude, the agreement in the frequency dependence and the positions of the structure function peaks may yield valuable information. Fitting the polydisperse structure function model introduced in Section II to the histologically estimated structure function model yielded reasonable cell radius estimates. The best-fit curves were plotted against the histologically estimated curves in Fig. 2. The estimated mean cell radii were 6.5, 6.5, and 7.5 μm for CHO, MAT and 4T1, respectively, which were within 16% error compared to the direct light microscope measures on live cells (6.7, 7.3, and 8.9 μm for CHO, MAT and 4T1, respectively; see Fig. 4 of [20]). The cell radii were slightly underestimated for all cases, probably because 2D histology was used instead of 3D, and because of cell shrinkage during fixing.

In conclusion, the structure function is required for accurately modeling the acoustic scattering in dense medium. The acoustically estimated structure function is related to the scatterer position distribution determined from histology.

ACKNOWLEDGMENT

The authors would like to thank Jamie R. Kelly for fabricating the cell pellet biophantoms.

REFERENCES

[1] A. Sadeghi-Naini, N. Papanicolau, O. Falou, J. Zubovits, R. Dent, S Verma, M. Trudeau, J. F. Boileau6, J. Spayne, S. Iradji, E. Sofroni, J. Lee, S. Lemon-Wong, M. Yaffe, M. C. Kolios, and G. J. Czarnota, "Quantitative ultrasound evaluation of tumor cell death response in locally advanced breast cancer patients receiving chemotherapy," Clin. Cancer Res., vol. 19, pp. 2163–2174, 2013.

[2] M. P. Andre, A. Han, E. Heba, J. Hooker, R. Loomba, C. B. Sirlin, J. W. Erdman, Jr. and W. D. O'Brien, Jr., "Accurate diagnosis of nonalcoholic fatty liver disease in human participants via quantitative ultrasound," in IEEE Int. Ultrason. Symp. Proc., 2014, pp. 2375–2377.

[3] S. C. Lin, E. Heba, T. Wolfson, B. Ang, A. Gamst, A. Han, J. W. Erdman, W. D. O'Brien, Jr., M. P. Andre, C. B. Sirlin, and R. Loomba, "Noninvasive diagnosis of nonalcoholic fatty liver disease and quantification of liver fat using a new quantitative ultrasound technique," Clin. Gastroenterol H., vol. 13, no. 7, pp. 1337–1345, 2015.

[4] H. Tadayyon, A. Sadeghi-Naini, L. Wirtzfeld, F. C. Wright, and G. Czarnota, "Quantitative ultrasound characterization of locally advanced breast cancer by estimation of its scatterer properties," Med. Phys., vol. 41, no.1, pp. 012903, 2014.

[5] F. L. Lizzi, M. Ostromogilsky, E. J. Feleppa, M. C. Rorke, and M. M. Yaremko, "Relationship of ultrasonic spectral parameters to features of tissue microstructure," IEEE Trans. Ultrason. Ferroelect. Freq. Contr., vol. 33, pp. 319–329, 1986.

[6] M. F. Insana, R. F. Wagner, D. G. Brown, and T. J. Hall, "Describing small-scale structure in random media using pulse-echo ultrasound," J. Acoust. Soc. Am., vol. 87, no. 1, pp. 179–192, 1990.

[7] M. L. Oelze and W. D. O'Brien, Jr., "Application of three scattering models to characterization of solid tumors in mice," Ultrason. Imaging, vol. 28, no. 2, pp. 83–96, 2006.

[8] M. Teisseire, A. Han, R. Abuhabsah, J. P. Blue, Jr., S. Sarwate, and W. D. O'Brien, Jr., "Ultrasonic backscatter coefficient quantitative estimates from Chinese hamster ovary cell pellet biophantoms," J. Acoust. Soc. Am., vol. 128, pp. 3175–3180, 2010.

[9] A. Han, R. Abuhabsah, J. P. Blue, Jr., S. Sarwate, and W. D. O'Brien, Jr., "Ultrasonic backscatter coefficient quantitative estimates from high-concentration Chinese hamster ovary cell pellet biophantoms," J. Acoust. Soc. Am., vol. 130, pp. 4139–4147, 2011.

[10] A. Han, R. Abuhabsah, R. J. Miller, S. Sarwate, W. D. O'Brien, Jr., "The measurement of ultrasound backscattering from cell pellet biophantoms and tumors ex vivo," J. Acoust. Soc. Am., vol. 134, no. 1, pp. 686–693, 2013.

[11] R. M. Vlad, R. K. Saha, N. M. Alajez, S. Ranieari, G. J. Czarnota and M. C. Kolios, "An increase in cellular size variance contributes to the increase in ultrasound backscatter during cell death," Ultrasound in Med. Biol., vol. 9, pp. 1546–1558, 2010.

[12] V. Twersky, "Low-frequency scattering by correlated distributions of randomly oriented particles," J. Acoust. Soc. Am., vol. 81, no. 5, pp. 1609–1618, 1987.

[13] V. Twersky, "Low-frequency scattering by mixtures of correlated nonspherical particles," J. Acoust. Soc. Am., vol. 84, no. 1, pp. 409–415, 1988.

[14] I. Fontaine, M. Bertrand, and G. Cloutier, "A system-based approach to modeling the ultrasound signal backscattered by red blood cells," Biophysical Journal, vol. 77, pp. 2387–2399, 1999.

[15] D. Savéry and G. Cloutier, "A point process approach to assess the frequency dependence of ultrasound backscattering by aggregating red blood cells," J. Acoust. Soc. Am., vol. 110, no. 6, pp. 3252–3262, 2001.

[16] E. Franceschini, R. K. Saha, and G. Cloutier, "Comparison of three scattering models for ultrasound blood characterization," IEEE Trans. Ultrason. Ferroelectr. Freq. Control, vol. 60, no. 11, pp. 2321–2334, 2013.

[17] J. K. Percus and G. J. Yevick, "Analysis of classical statistical mechanics by means of collective coordinates," Phys. Rev., vol. 110, pp. 1–13, 1958.

[18] E. Franceschini and R. Guillermin, "Experimental assessment of four ultrasound scattering models for characterizing concentrated tissue-mimicking phantoms," J. Acoust. Soc. Am., vol. 132, no. 6, pp. 3735–3747, 2012.

[19] E. Franceschini, R. Guillermin, F. Tourniaire, S. Roffino, E. Lamy and J.-F. Landrier, "Structure Factor Model for understanding the measured backscatter coefficients from concentrated cell pellet biophantoms," J. Acoust. Soc. Am., vol. 135, no. 6, pp. 3620-3631, 2014.

[20] A. Han and W. D. O'Brien, Jr., "Structure function for high-concentration biophantoms of polydisperse scatterer sizes," IEEE Trans. Ultrason. Ferroelectr. Freq. Control, vol. 62, no. 2, pp. 303–318, 2015.